Clustered *de novo* start-loss variants in *GLUL* result in a developmental and epileptic encephalopathy via stabilization of glutamine synthetase

Graphical abstract

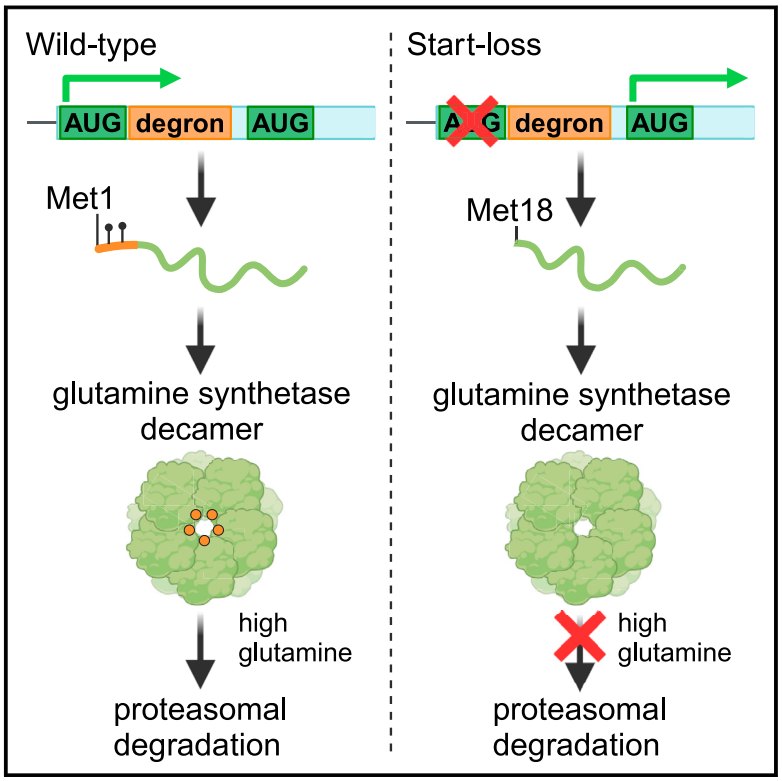

Authors

Amy G. Jones, Matilde Aquilino, Rory J. Tinker, ..., Gregory Gimenez, Takashi Namba, Stephen P. Robertson

Correspondence

stephen.robertson@otago.ac.nz

Start-loss variants in *GLUL* result in a severe developmental and epileptic phenotype through the stabilization of glutamine synthetase, an enzyme crucial for brain function. This disorder is unusual in its gain-of-stabilization mechanism contrasting with the allelic deficiency disorder.

Jones et al., 2024, The American Journal of Human Genetics *111*, 729–741
April 4, 2024
https://doi.org/10.1016/j.ajhg.2024.03.005

Clustered *de novo* start-loss variants in *GLUL* result in a developmental and epileptic encephalopathy via stabilization of glutamine synthetase

Amy G. Jones,[1] Matilde Aquilino,[2] Rory J. Tinker,[3] Laura Duncan,[4] Zandra Jenkins,[1] Gemma L. Carvill,[5] Stephanie J. DeWard,[6] Dorothy K. Grange,[7] MJ Hajianpour,[8] Benjamin J. Halliday,[1] Muriel Holder-Espinasse,[9] Judit Horvath,[10] Silvia Maitz,[11] Vincenzo Nigro,[12] Manuela Morleo,[12] Victoria Paul,[10] Careni Spencer,[13,14] Alina I. Esterhuizen,[13,15,16] Tilman Polster,[17] Alice Spano,[18] Inés Gómez-Lozano,[2] Abhishek Kumar,[19] Gemma Poke,[20] John A. Phillips III,[3] Hunter R. Underhill,[21] Gregory Gimenez,[22] Takashi Namba,[2] and Stephen P. Robertson[1,*]

Summary

Glutamine synthetase (GS), encoded by *GLUL*, catalyzes the conversion of glutamate to glutamine. GS is pivotal for the generation of the neurotransmitters glutamate and gamma-aminobutyric acid and is the primary mechanism of ammonia detoxification in the brain. GS levels are regulated post-translationally by an N-terminal degron that enables the ubiquitin-mediated degradation of GS in a glutamine-induced manner. GS deficiency in humans is known to lead to neurological defects and death in infancy, yet how dysregulation of the degron-mediated control of GS levels might affect neurodevelopment is unknown. We ascertained nine individuals with severe developmental delay, seizures, and white matter abnormalities but normal plasma and cerebrospinal fluid biochemistry with *de novo* variants in *GLUL*. Seven out of nine were start-loss variants and two out of nine disrupted 5′ UTR splicing resulting in splice exclusion of the initiation codon. Using transfection-based expression systems and mass spectrometry, these variants were shown to lead to translation initiation of GS from methionine 18, downstream of the N-terminal degron motif, resulting in a protein that is stable and enzymatically competent but insensitive to negative feedback by glutamine. Analysis of human single-cell transcriptomes demonstrated that *GLUL* is widely expressed in neuro- and glial-progenitor cells and mature astrocytes but not in post-mitotic neurons. One individual with a start-loss *GLUL* variant demonstrated periventricular nodular heterotopia, a neuronal migration disorder, yet overexpression of stabilized GS in mice using *in utero* electroporation demonstrated no migratory deficits. These findings underline the importance of tight regulation of glutamine metabolism during neurodevelopment in humans.

Introduction

Multiple monogenic disorders that disrupt the metabolism of amino acids have been described, many of which manifest as developmental encephalopathies.[1] The pathogenic mechanisms underlying these disorders are diverse, acting via gain of function, loss of function, or altered metabolic flux, which results in high, low, or maldistribution of amino acids within and between subcellular compartments. Genes implicated in these conditions encode enzymes, transporters, or receptors and usually result in a deficiency state, although some conditions are monogenic gain-of-function disorders.[2–6]

Glutamine metabolism contributes to multiple roles in nervous system function. First, glutamine is a precursor of the neurotransmitters gamma-aminobutyric acid (GABA) and glutamate. Glutamate released from neurons is rapidly removed from the synaptic cleft by astrocytes through excitatory amino acid transporters and is then converted to glutamine within adjacent astrocytes by glutamine synthetase (GS). Astrocytes then secrete glutamine that is taken up by presynaptic neurons through sodium-coupled neutral amino acid transporters to establish a pool of neuronal glutamine for the conversion to glutamate and GABA. This interaction is termed the glutamate-glutamine couple.[7,8] Second, the conversion of

[1]Department of Women's and Children's Health, Dunedin School of Medicine, University of Otago, Dunedin, New Zealand; [2]Neuroscience Center, HiLIFE – Helsinki Institute of Life Science, University of Helsinki, Helsinki, Finland; [3]Vanderbilt University Medical Center, Nashville, TN, USA; [4]Center for Individualized Medicine, Mayo Clinic, Jacksonville, FL, USA; [5]Department of Neurology, Feinberg School of Medicine, Northwestern University, Chicago, IL, USA; [6]GeneDx, Gaithersburg, MD, USA; [7]Washington University, St. Louis, Missouri, USA; [8]Albany Medical College, Albany, NY, USA; [9]Department of Clinical Genetics, Guys Hospital, London, UK; [10]Münster University Hospital, Münster, Germany; [11]Medical Genetics Service, Oncology Department of Southern Switzerland, Ente Ospedaliero Cantonale, Lugano, Switzerland; [12]Department of Precision Medicine, University of Campania "Luigi Vanvitelli," Naples, Italy; [13]Division of Human Genetics, Department of Pathology, Faculty of Health Sciences, University of Cape Town, Cape Town, South Africa; [14]Department of Medicine, Division of Human Genetics, Groote Schuur Hospital, Cape Town, South Africa; [15]Neuroscience Institute, University of Cape Town, Cape Town, South Africa; [16]National Health Laboratory Service, Groote Schuur Hospital, Cape Town, South Africa; [17]Department of Epileptology (Krankenhaus Mara, Bethel Epilepsy Center) Medical School OWL, Bielefeld University, Bielefeld, Germany; [18]Maggiore Della Carità Hospital, Novara, Italy; [19]Centre for Protein Research, University of Otago, Dunedin, New Zealand; [20]Genetics Health Service New Zealand, Wellington Hospital, Wellington, New Zealand; [21]University of Utah, Salt Lake City, UT, USA; [22]Department of Pathology, Dunedin School of Medicine, University of Otago, Dunedin, New Zealand

*Correspondence: stephen.robertson@otago.ac.nz
https://doi.org/10.1016/j.ajhg.2024.03.005.

glutamate to glutamine catalyzed by GS is the major mechanism of ammonia removal in the brain.[9] Third, glutamine can enter the tricarboxylic acid cycle via glutaminolysis to supplement cellular energy production.[10] Recently, glutaminolysis has been shown to be necessary for neural progenitor expansion in the human fetal neocortex.[11]

GS (PDB: 2OJW) is encoded by *GLUL* (OMIM: 138290). GS subunits, each with a molecular weight of 42 kilodaltons (kDa), are assembled in the cytoplasm into a cylindrical decamer that constitutes the active, multimeric form of the enzyme. Reflecting its role in ammonia detoxification, GS is highly expressed in the liver, kidneys, and the central nervous system with a preponderance in glial cell types but not neurons. A GS deficiency disorder (OMIM: 610015) has previously been reported in four individuals with developmental delay, seizures, and low plasma and cerebrospinal fluid glutamine and ammonia levels. The genetic basis for this condition is biallelic hypomorphic missense variants substituting residues at the active site interface of GS.[12–15] Notably, knockout *Glul* mice exhibit embryonic lethality at embryonic day (E) 3.5, which is indicative of an essential role for GS in early embryogenesis.[16]

Tissue glutamine levels have been suggested to be regulated, in part, through an autoregulatory negative feedback mechanism where elevated glutamine acts on GS subunits, leading to their ubiquitin-mediated proteasomal degradation. Following exposure of cells to glutamine, an N-terminal degron is acetylated by p300/CREB binding protein and subsequently recognized and ubiquitinated by $CRL4^{CRBN}$, resulting in proteasomal degradation.[17] The developmental consequences of perturbations of this autoregulatory feedback mechanism are currently unknown.

Here, we describe a cohort of individuals with severe neurodevelopmental phenotypes who were all heterozygous for variants that disrupt the canonical start codon in *GLUL* either directly via start-loss variants or through splice site variants that result in splice exclusion of the start codon. Translation of GS from these variant transcripts is maintained using a downstream alternative start site resulting in truncated GS that is stable and enzymatically competent but insensitive to negative feedback by glutamine. This disorder of glutamine metabolism illustrates the importance of the regulation of GS activity during human neurodevelopment to maintain glutamine levels within a tightly specified range.

Material and methods

Individual recruitment, ethics, and variant discovery

Each participating laboratory performed sequencing on probands under ethics approved by the corresponding institutions. The observation of variants in *GLUL* lead to this collaboration facilitated by GeneMatcher.[18] All participating families provided signed consent (Otago Ethics 13/STH/56). Following exome sequencing, Sanger sequencing was used to confirm the observed variant. Parental analysis was performed in eight probands for *de novo* analysis. Parentage and the *de novo* status were confirmed in eight out of nine probands via trio exome sequencing.

Cell lines

HEK293FT cells (Life Technologies) were maintained in DMEM media (Gibco, #11995040) supplemented with 2% (v/v) penicillin/streptavidin (Gibco, #15140122) and 10% (v/v) fetal bovine serum (FBS) (Moregate Biotech, #FBSF) at 37°C in 5% CO_2.

HEK293_GLULKO_20, hereafter referred to as HEK293_GLULKO, a HEK293FT *GLUL* CRISPR knockout cell line was used under license (Accelerate Technologies[19]). Cells were maintained in DMEM media (Gibco, #11995040) supplemented with 2% (v/v) penicillin/streptavidin (Gibco, #15140122), 10% (v/v) FBS (Moregate Biotech, #FBSF), and 2 mM L-glutamine (Gibco, #25030081).

Start-loss and control fibroblast cell lines were cultured in DMEM media (Gibco, #11995040) supplemented with 2% (v/v) penicillin/streptavidin (Gibco, #15140122) and 10% (v/v) FBS (Moregate Biotech, #FBSF).

Antibodies

Primary antibodies used in immunoblotting experiments were mouse anti-FLAG (1:7000, Sigma, #F3165), rabbit anti-GAPDH (1:3000, Sigma, #G9545), rabbit anti-beta-actin (1:5000, Cell Signaling Technology, #4970), and rabbit anti-GS (1:1000, Abcam, #ab197024). Secondary IRDye fluorescent antibodies IRDye 800CW goat anti-mouse (LI-COR, #926–32210), IRDye 800CW goat anti-rabbit (LI-COR, #926–32211), IRDye 680RD goat anti-mouse (LI-COR, #926–68070), and IRDye 680RD goat anti-rabbit (LI-COR, #926–68071) were used for western blot visualization.

RNA extraction

RNA was extracted using the Macherey-Nagel NucleoSpin RNA plus kit (Macherey-Nagel, #740984) and converted to cDNA using Superscript III Reverse Transcriptase (Invitrogen, #18080), 100 ng/μL random hexamers, 50 μM oligo$(dT)_{18}$, and 20 mM deoxyribonucleotide triphosphate (dNTP) in a 20 μL reaction.

Expression plasmids

Human GS (GenBank: NM_001033044.4) expression constructs with full length (GS_FL), start-loss variant c.1A>T (p.Met1?, GS_SL), 17 amino acid truncated (GS_met^{18}), 28 amino acid truncated (GS_met^{29}), enzymatically compromised variant c.970C>T (p.Arg324Cys, GS_p.Arg324Cys), and enzymatically compromised variant c.1021C>T (p.Arg341Cys, GS_p.Arg341Cys) were cloned into expression vectors with C-terminal tags. GS_FL, GS_SL, GS_met^{18}, GS_met^{29}, GS_p.Arg324Cys, and GS_p.Arg341Cys were cloned into pcDNA3.1/V5-His-TOPO with a 3xFLAG Twin-Strep-tag. GS_FL and GS_SL were cloned into pCAGGS with an HA-tag.

All GS fragments were amplified using Q5 Hi-Fidelity DNA polymerase (NEB #M0491) from HEK293FT cDNA and inserted at EcoRI and HindIII sites of appropriate plasmids using NEBuilder HiFi DNA assembly (NEB, #E2621). All expression constructs were confirmed with DNA sequencing.

Cell transfection

HEK293_GLULKO cells were transfected with 800 ng plasmid per well of a 24-well plate with 2 μL lipofectamine 2000 (Invitrogen, #11668019) following manufacturer's protocols for reverse transfection. Cells were cultured in DMEM supplemented with 10%

(v/v) FBS and 2 mM L-glutamine. The equivalent volume of DMEM media supplemented with 10% (v/v) FBS and 2 mM L-glutamine was added approximately 5 h post-transfection.

Western blotting

Cells were lysed in native conditions (PBS, 2.5% [v/v] Triton X- and cOmplete protease inhibitor [Roche, #04693132001]). Clarified lysates were heated at 95°C with 1× Laemmli protein loading dye. Between 10 and 20 μg of protein was loaded and separated on an SDS-PAGE gel and transferred to a nitrocellulose membrane. Following blocking in 5% (w/v) milk in 1× PBS, the western blot was incubated with primary antibodies at 4°C for 1 h or overnight. Secondary anti-mouse and anti-rabbit fluorescent antibodies, described above, were incubated at room temperature for 1 h and imaged on a LiCor odyssey.

Strep-tag affinity purification

Following transfection, cells were lysed in native buffer. Native buffer was composed of 1× cOmplete protease inhibitor (Roche, #04693116001) and prepared in 1× PBS and 2.5% (v/v) Triton X-100 was added immediately before use. Following clarification, 150–200 μL lysate was incubated with 20–50 μL MagStrep XT beads (IBA Lifesciences, #2-4090-022) for 1 h at 4°C. Following binding, beads were washed twice in 1× PBS with 1% (v/v) Triton X-100 and twice in 1× PBS.

Protein sequencing mass spectrometry

After enrichment of GS by Strep-tag affinity purification, proteins were on-bead digested with chymotrypsin. The eluted chymotryptic protein fragments were subjected to nano-flow liquid chromatography coupled tandem mass spectrometry using an LTQ Orbitrap XL mass spectrometer.

The resulting data were analyzed against an in-house FASTA sequence database containing the GS sequence using the SEQUEST-HT search engine within the Proteome Discoverer software (version 2.5) (Thermo Fisher Scientific, USA). Data were analyzed with no enzyme cleavage specified and the following dynamic and static modifications: oxidation of methionine (dynamic), deamidation of asparagine and glutamine (dynamic), and carbamidomethylation of cysteine (static). All fragment ion spectra assigned to the N-terminal peptides of the GS by the software were manually confirmed for correct peak assignment.

Cycloheximide assay

Following transfection, 12 h later all media were removed and replaced with glutamine-free DMEM (Gibco, #11960044) supplemented with 10 mM L-glutamine (high) or 1 mM L-glutamine (low) and 100 μg/mL cycloheximide (Sigma, #C4859) (treated) or 1.5 μL DMSO (Sigma, #D2438) (non-treated). Cells were lysed for western blot analysis 6 h later. Quantification of western blot bands was performed with ImageStudio software (LI-COR). All data were normalized to untreated full-length GS and the fold reduction calculated as the proportion of untreated to treated GS for each glutamine condition.

GS activity assay

Following transfection, GS was purified as described in Strep-tag affinity purification above, followed by elution with buffer BTX (IBA Lifesciences, #2-1042-025). A complete buffer exchange was performed with 30k molecular weight cutoff protein purification columns (Pierce, #88502) exchanging biotin elution buffer for GS assay buffer. Protein was measured on a Thermo Scientific NanoDrop spectrophotometer at A280, and equal concentrations were used in the subsequent activity assay. Samples were measured for GS activity using the GS activity assay kit colorimetric kit (Abcam, #ab284572) as per the manufacturer instructions.

Statistical analysis

Cycloheximide and activity assay data are presented as the mean +/− standard error of the mean. p values were calculated using an unpaired two-tailed Student's t test. Immunoblot data from subject-derived fibroblasts were analyzed with the Shapiro-Wilk test to test normality. p values were calculated with a one-way ANOVA, and post-hoc testing was done using the Tukey method. Significance was described as *$p < 0.05$, **$p < 0.01$, and not statistically significant (NS).

Single-cell RNA-sequence analysis

Single-cell and single-nucleus RNA sequencing (RNA-seq) data were obtained from published datasets GEO: GSE168408[20] and GEO: GSE144462.[21]

The R package Seurat (v.4.0.5) was used for clustering and expression analysis.[22,23] Cells with mitochondrial gene counts >10% and ribosomal gene counts >20% were excluded, followed by normalization using the LogNormalize method. The most variable genes were found with the variance-stabilizing transformation selection method. Data were scaled and dimensionality reduced with principal component analysis, which was further visualized with the RunUMAP function using the first 10 principal components. Cells were clustered using a resolution of 0.5, and clusters were manually annotated based on markers used in the original publications.[20,21] FeaturePlot and VlnPlot functions were used to visualize *GLUL* expression across cell clusters.

In utero electroporation of embryonic mouse neocortex

All the experiments involving *in utero* electroporation (IUE) were performed in accordance with the Directive 2010/63/EU and approved by National Animal Experiment Board, Finland (license number ESAVI/15112/2021). IUE was performed as previously described.[24] Pregnant C57BL/6JRj mice received analgesic buprenorphine (0.03 mg/kg body weight) 30 min prior to surgery at E13.5 or E16.5 following anesthesia with isoflurane (3% induction, 2%–1.5% maintenance). pCAGGS plasmids (1 μg/μL; empty vector as a control, GS_FL or GS_SL) together with pCAGGS-EGFP (0.3 μg/μL) and 0.1% Fast Green were injected intraventricularly into the lateral ventricle of the embryos with a glass capillary, followed by electroporation (five 50-ms square pulses of 40 V with 950-ms intervals). Mice received anti-inflammatory carprofen (10 mg/kg body weight) and were monitored three days after the surgery. Mice were sacrificed and embryos were harvested two or five days post-electroporation. The embryonic brains were dissected and A13 paraformaldehyde (PFA) fixed for immunohistochemistry as described below.

Immunohistochemistry

For immunohistochemistry, 14 μm thick coronal sections were treated with 0.01 M citrate buffer at 70°C for 60 min for antigen retrieval followed by incubation at room temperature for 20 min. The sections were then permeabilized by 1% (v/v) Triton X-100/PBS for 30 min, followed by incubation with 0.1 M Glycine/PBS for 30 min at room temperature. Subsequently, the sections were incubated with TX buffer (0.2% gelatin, 300 mM

NaCl, 0.3% Triton X-100 in PBS) containing the primary antibodies listed below over night at 4°C. Sections were washed with PBS followed by incubation with a mixture of appropriate secondary antibodies in TX buffer, which also contains DAPI (1:1000, Sigma). The primary antibodies were mouse chicken anti-GFP (1:500, Aves, GFP-1020), rat anti-CTIP2 (1:200, ab18465, Abcam), mouse anti-Olig2 (1:200, MABN50, Chemicon), rat anti-Pax6 (1:200, 939802, BioLegend), mouse anti-SATB2 (1:200, ab51502, Abcam), goat anti-Sox2 (1:500, AF2018, R&D systems), and rabbit anti-Tbr2 (1:500, ab23345, Abcam). Secondary antibodies made in donkey were anti-chicken IgY Alexa 488 (1:500, 703-545-155, Jackson ImmunoResearch), anti-goat IgG Alexa 647 (1:500, 705-605-147, Jackson ImmunoResearch), anti-mouse IgG Cy3 (1:200, Jackson 715-165-151, Jackson ImmunoResearch), anti-rabbit IgG Alexa 647 (1:500, 711-545-152, Jackson ImmunoResearch), anti-rat IgG Alexa 647 (1:500, 712-605-153, Jackson ImmunoResearch), and anti-rat IgG Cy3 (1:200, 712-165-153, Jackson ImmunoResearch).

Image acquisition and quantifications

All images were acquired by Zeiss LSM 780 scanning confocal microscope with C-Apochromat 40×/1.20 W Korr water objective. z stack images with 1.2 μm optical sections were taken. All images were analyzed and processed with ZEN (Zeiss) and FIJI (ImageJ). Data were processed by Excel (Microsoft), and results were plotted in Prism (GraphPad Software).

Results

Start-loss variants in *GLUL* cause a developmental and epileptic encephalopathy phenotype

A cohort of nine probands who were clinically evaluated at diagnostic centers in New Zealand, North America, Europe, and South Africa were assembled through GeneMatcher[18] as having monoallelic variants in *GLUL*. All individuals had exome sequencing performed either as part of their clinical diagnostic evaluation or part of a research protocol. No individual (age range 16 months–16 years) had a history of parental consanguinity or a family history of epilepsy, developmental delay, or intellectual disability. On clinical assessment, a consistent phenotype of drug-resistant epilepsy, global developmental delay, and hypotonia was present in all individuals (Table 1). All individuals were eumorphic. The epilepsy was characterized as generalized (n = 4), combined general and focal (n = 3), focal (n = 1), or unknown (n = 1). Most individuals had a developmental and epileptic encephalopathy, with one individual meeting diagnostic criteria for infantile epileptic spasms syndrome. Developmental delays were severe to profound and affected all domains of development in all individuals. Biochemical analysis demonstrated normal plasma (n = 6) and cerebrospinal fluid (n = 4) glutamine levels. Three individuals had serum ammonia measured in the normal range. Brain magnetic resonance imaging (MRI) identified enlarged perivascular spaces in five probands and hypomyelination in seven instances.

Analysis of whole-exome sequencing datasets revealed heterozygous variants in the 5′ region of *GLUL* in all nine probands (Table 1; Figure 1A). One individual's genotype, individual 3, was previously reported[25] as part of the exome sequencing of a cohort of 202 individuals with periventricular nodular heterotopia. The project identified the *de novo GLUL* variant, c.1A>C, and assigned it as a variant of uncertain significance.[25]

Parental testing was conducted in eight families, with the *GLUL* variant shown to be *de novo* in all evaluated individuals. *De novo* status could not be confirmed for individual 5. Seven individuals had heterozygous start-loss variants within the initiation codon of *GLUL*: GenBank: NM_001033044.4 (c.3G>A [p.Met1?]), GenBank: NM_001033044.4 (c.1A>T [p.Met1?]), GenBank: NM_001033044.4 (c.1 A>C [p.Met1?]), and GenBank: NM_001033044.4 (c.1A>G [p.Met1?]). Two individuals (individuals 7 and 8) were heterozygous for intronic variants: GenBank: NM_001033044.4 (c.−13−1G>A [p.?]) and GenBank: NM_001033044.4 (c.−13−2A>G [p.?]), located upstream of a *GLUL* 5′-UTR splice site (Figure 1A). All variants were absent from gnomAD (v.3.1.2), and variant c.1A>G (n = 4) was recurrent in this cohort.

Splice prediction software, SpliceAI,[26] predicted loss of the splice acceptor site immediately downstream of the c.−13−1G>A and c.−13−2A>G variants with high confidence (delta score = 1.0). In both instances, a new acceptor site was predicted to lie 26 bp 3′ from the intron/exon boundary site, also with high confidence (delta score = 0.97), and if deployed was anticipated to truncate the first four amino acids of GS and excise the canonical translational start site of *GLUL* (Figure 1B). To corroborate these predictions, RNA from cultured dermal fibroblasts from an individual with the intronic *GLUL* variant c.−13−2A>G was isolated. Following cDNA preparation, a 357-bp amplicon spanning the 5′ UTR exon 2/coding exon 2 junction was PCR amplified and sequenced. An alternatively spliced transcript was identified that excluded 26 bp, spanning 5′ UTR exon 2 and the first 13 bases of coding exon 1, including the canonical initiation codon (Figure 1B).

Collectively, these data predict that the individuals with either start site or splice variants have a non-functional canonical translational start site. The recurrent observation of these highly localized *de novo GLUL* variants associated with very similar phenotypes in all nine individuals studied strongly supports their pathogenicity. However, the prior description of an autosomal-recessive disorder at the same locus without phenotypic manifestations in heterozygotes[12–15] implies that the functional effect of the alleles described above must be distinct from the previously reported loss-of-function mechanism.

Start-loss variants in *GLUL* result in initiation of translation at met[18]

As *de novo* monoallelic variants in the 5′ region of *GLUL* are associated with a severe neurodevelopmental phenotype yet heterozygotes for *GLUL* deficiency alleles are neurologically normal, we hypothesized that the transcript

Table 1. Clinical and genetic characteristics of individuals with *GLUL* variants

Individual	1	2	3	4	5	6	7	8	9
GLUL variant GenBank: NM_001033044.4 (GenBank: NP_001028216.1)	c.3G>A p.Met1?	c.1A>T p.Met1?	c.1A>C p.Met1?	c.1A>G p.Met1?	c.1A>G p.Met1?	c.1A>G p.Met1?	c.−13−1G>A p.?	c.−13−2A>G p.?	c.1A>G p.Met1?
De novo status	+	+	+	+	unknown	+	+	+	+
Region	USA	USA	UK	RSA	USA	USA	Italy	USA	Germany
Sex	female	female	female	female	female	female	female	female	female
Biochemistry									
Plasma glutamine	normal	borderline low	unknown	normal	normal	normal	borderline low	normal	normal
Cerebrospinal fluid glutamine	low	normal	unknown	unknown	normal	normal	high	normal	low
Ammonia	normal	normal	unknown	normal	unknown	unknown	unknown	unknown	unknown
Cerebrospinal fluid neurotransmitters	unknown	normal	unknown	unknown	unknown	unknown	unknown	unknown	normal
Epilepsy									
Age of seizure onset	2 months	8 months	unknown	10 weeks	8 months	6 months	11 months	22 months	2 months
Seizure type	GTCS	focal, generalized	unknown	tonic, focal clonic, myoclonic atonic, GTCS	GTCS	tonic, myoclonic, GTCS	GTCS	myoclonic, GTCS, absence	epileptic spasms, focal clonic, focal myoclonic
Epilepsy type	generalized	combined focal and generalized	unknown	combined focal and generalized	generalized	combined focal and generalized	generalized	generalized	focal
Developmental and epileptic encephalopathy	yes	likely	unknown	yes	yes	yes	yes	yes	yes (infantile epileptic spasms syndrome)
Electroencephalogram findings	generalized paroxysmal fast activity; generalized slow spike-wave discharges (awake EEG)	focal electroclinical seizure; persistent hemispheric asymmetry; no interictal epileptiform features	not available	generalized encephalopathy with slow spike and wave	encephalopathic	several GTCS captured; multifocal discharges; encephalopathic background	disorganized; generalized slowing	frequent myoclonic seizures; generalized spike and wave	hypsarrhythmia
Seizure frequency	daily	1–6 per week	unknown	multiple daily	not available	daily	sporadic	50–100 per day	1–2 per month
Treatment response	refractory	ketogenic diet[a]	unknown	refractory	refractory	refractory	unknown	refractory	refractory
Global developmental delay	+	+	+	+	+	+	+	+	+
Neuroimaging									
Prominent perivascular spaces and thinning corpus callosum	+	+	unknown	+	−	−	+	unknown	+
Demyelination/hypomyelination	+	+	unknown	+	+	+	+	unknown	+

GTCS, generalized tonic-clonic seizure.
[a]Individual 2 on 4:1 ketogenic diet reduced seizures from 1–6 episodes per week to infrequent (1 episode every several months).

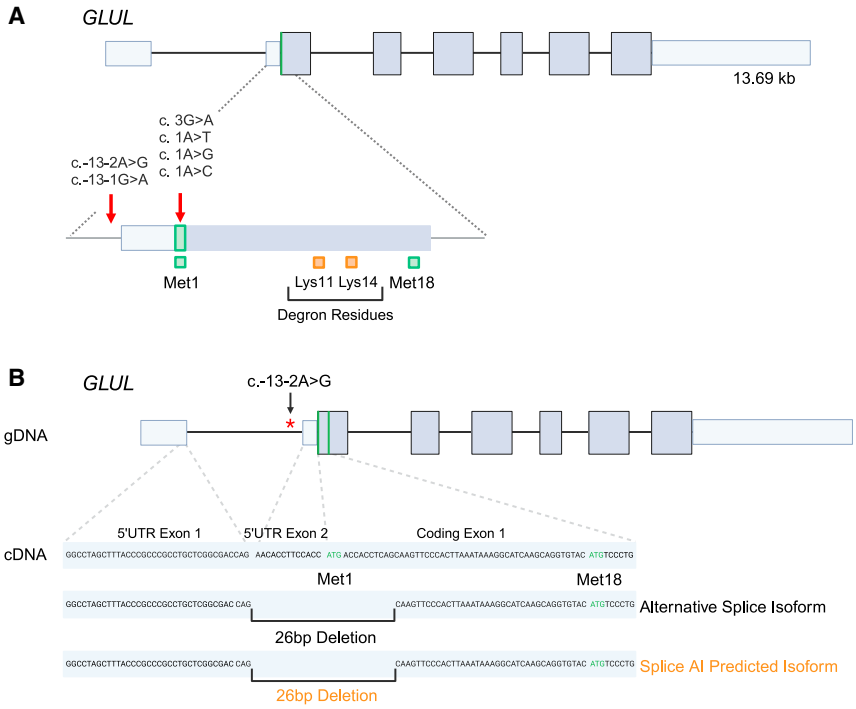

Figure 1. *GLUL* start-loss and splice site variant location

(A) Schematic of *GLUL* gene structure. The location of individual start-loss and splice variants are indicated relative to the first ATG (Met1) (green); variant c.1A>G (n = 4) was recurrent in this cohort. Key methionine amino acid residues (green) and lysine amino acid residues of the degron motif (orange) are indicated.

(B) An intronic variant in *GLUL* disrupts 5′ UTR splicing resulting in a 26 base pair deletion. Splice AI predicted a deletion of 26 base pairs resulting in the exclusion of 5′ UTR exon 2 and the first 13 base pairs of coding exon 1 (orange). Sequencing of dermal fibroblast RNA with c.−13−2A>G variant demonstrated an alternatively spliced isoform with a 26 base pair deletion, which removed 13 base pairs of 5′ UTR exon 2 and 13 base pairs of coding exon 1 and therefore excised the canonical start site. Dark boxes, coding exons; light boxes, UTR exons.

produced from the allele with 5′ *GLUL* variants exerts an effect distinct from loss of function. As *GLUL* transcripts were produced from both the full-length and splice variant allele (Figure 1B), we tested whether the start-loss and splice variant alleles produced detectable protein. Start-loss variants can result in loss of function or translational initiation from an alternative downstream codon. Western blotting of lysates from two start-loss and one splice variant fibroblast cell lines (derived from individuals 1, 6, and 8) and sex- and aged-matched controls was performed with anti-GS and anti-GAPDH antibodies. Western blots demonstrated that a second, smaller GS band was present in fibroblasts from individuals heterozygous for start-loss and splice variants, which was absent in control fibroblasts (Figure 2A). The difference in size between the two protein bands was estimated to be no larger than 4 kDa. Additionally, cloned *GLUL* expression constructs with start-loss variants migrated at a lower molecular weight than full-length GS on a western blot (Figure 2B). These data suggest that GS start-loss variants precipitate the utilization of an alternative downstream initiation site.

Because variant alleles produce a detectable protein product, we sought to confirm from where translation of the smaller GS product is initiated. There are two candidate methionine residues that are within the predicted size distance of 4 kDa (Figure 2), located at positions 18 (met^{18}) and 29 (met^{29}) in GS. Translation from both met^{18} and met^{29} is predicted to result in the loss of 2 kDa and 3 kDa, respectively, from full-length GS. To determine the translation initiation site of GS from transcripts with start-loss variants, the protein sequence of GS produced from variant alleles was determined by mass spectrometry. Expression constructs of GS_FL, GS_SL, GS_met^{18}, and GS_met^{29}were investigated. All *GLUL* constructs were successfully expressed and protein visualized by western blotting (Figures 2C and S1).

Following transfection and affinity purification, peptides generated by chymotryptic digestion were analyzed by tandem mass spectrometry (MS/MS). The peptide detected nearest to the N terminus of GS_FL spanned residues 9–17 (Figure 2D). In this instance, the N-terminal sequence coverage was incomplete, and no peptide encompassing residues 1–8 was detected. The most proximal N-terminal peptide detected from both GS_met^{18} and GS_SL spanned residues 20–30 (Figure 2D). The first N-terminal peptide of GS_met^{29} did not align with the sequence of the N terminal of GS_SL (Figure S1). The observation that the N-terminal protein sequence of GS_SL aligns directly with GS_met^{18} is consistent with the start-loss transcript initiating at met^{18}.

Met^{18} GS is stabilized in the presence of high glutamine compared to full-length GS

We next sought to determine the consequences of truncated GS translated from met^{18}. Our data indicates that truncated GS is stable (Figures 2A, 2B, and 2C), but quantitative evidence for this is lacking. The truncation of the first 17 amino acids results in the loss of degron residues lysine 11 and 14 (Figure 1A).[17,27] Under high-glutamine conditions, these two lysine residues are acetylated, triggering ubiquitin-mediated proteasomal degradation.[17] Due to the loss of the glutamine-sensitive degron sequence, it is possible that truncated GS is stabilized

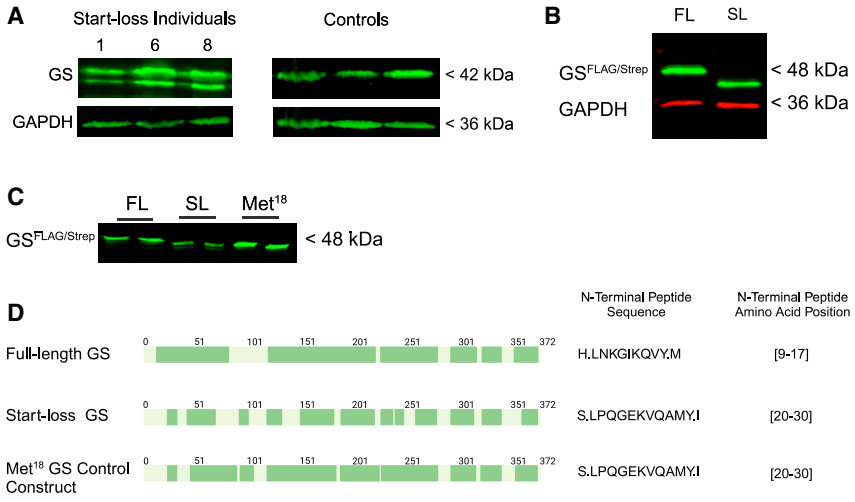

Figure 2. Start-loss variants in *GLUL* result in initiation of translation at methionine[18]

(A) Fibroblasts from individuals heterozygous for *GLUL* start-loss variants produce two GS isoforms. Lysates were prepared from three fibroblast cell lines from individuals heterozygous for start-loss variants (individuals 1, 6, and 8) and sex- and age-matched fibroblast controls. Western blotting was performed with GS and GAPDH antibodies (n = 3).

(B) Full-length GS migrates at a higher molecular weight than start-loss GS. Full-length $GS^{FLAG/Strep}$ and start-loss $GS^{FLAG/Strep}$ expression constructs were transfected into HEK293_GLULKO cells. Cell extracts were probed by western blotting with FLAG and GAPDH antibodies (n = 3).

(C) Full-length, start-loss, and methionine[18] control GS expression constructs are stably expressed. Full-length, start-loss, and met^{18} $GS^{FLAG/Strep}$ expression constructs were individually transfected into HEK293_GLULKO cells. Cell extracts were analyzed by western blotting with FLAG antibodies and duplicate wells were loaded.

(D) N-terminal start-loss GS sequence aligns with GS_met^{18} sequence. GS expression constructs were transfected in HEK293_GLULKO cells. Following affinity purification and chymotrypsin enzymatic digestion, peptides were identified by MS/MS. Identified sequences are shown as dark green boxes. The most N-terminal peptide sequence and amino acid peptide positions are indicated. FL, full-length; SL, start-loss c.1A>T variant; met^{18}, first 17 amino acids truncated.

compared to full-length GS, attributable to the loss of glutamine-mediated degradation.

To assess the stability of truncated GS, C-terminal-tagged GS_FL and GS_met^{18} constructs were transfected into HEK293_GLULKO cells[19] and cultured in low L-glutamine (1 mM). Protein synthesis was blocked with the addition of cycloheximide, and after a 6-h incubation, GS levels were measured by quantitative western blot analysis after immunostaining for the cognate protein tags. Fold reductions in GS levels were calculated as the proportion of GS in DMSO-treated negative controls relative to the proportion of GS treated with cycloheximide (Figure 3A). The average fold reduction in low glutamine was approximately the same for both GS_FL and GS_met^{18} (average fold reduction +/− SEM; GS_FL 1.56 ± 0.13 and GS_met^{18} 1.51 ± 0.10) (Figure 3C), indicating that under low glutamine conditions, GS_met^{18} is as stable as GS_FL.

We then sought to determine the effect of glutamine on truncated GS because it is missing key glutamine-sensitive degron residues and is hence predicted to be insensitive to glutamine-mediated degradation. To test this, GS_FL and GS_met^{18} transfections were treated with cycloheximide and cultured in high (10 mM) or low (1 mM) glutamine (Figures 3A and 3B).

Full-length GS had an average fold reduction of 2.97 ± 0.38 in high glutamine compared to 1.56 ± 0.13 in low glutamine and was significantly different between glutamine conditions ($p = 0.013$, Figure 3C). The higher fold reduction of full-length GS in high-glutamine conditions demonstrates increased GS degradation compared to that occurring in low-glutamine conditions. This finding is consistent with the presence and effect of the glutamine-sensitive degron in full-length GS. In contrast, the GS_met^{18}-fold reduction in high glutamine was 1.90 ± 0.31 and in low glutamine was 1.51 ± 0.10, which are not statistically different ($p = 0.27$, Figure 3C), indicating that the GS_met^{18} is insensitive to glutamine-mediated degradation. To corroborate these findings, dermal fibroblasts from individuals 1, 6, and 8 were cultured in low and high glutamine levels, and as seen in the transfection-based experiments, GS levels were stabilized when glutamine levels were elevated (Figures 3D and 3E). Interestingly, the amount of not only the truncated GS but also the full-length GS in these subject-derived fibroblasts did not reduce significantly with the high-glutamine condition compared to low glutamine, suggesting that the truncated GS stabilizes the entire GS decamer complex, which would presumptively consist of full-length and truncated GS monomers (Figures 3D and 3E).

Collectively, these findings show that truncated GS has comparable stability to that of full-length GS in low-glutamine conditions, but when glutamine levels are raised, full-length GS undergoes degradation while truncated GS is stabilized due to a lack of glutamine-sensitive degradation.

Met[18] GS retains enzymatic activity comparable to full-length GS

It is unclear whether truncated GS has retained its enzymatic capability. It is possible that the N-terminal truncated GS, after incorporation into decamer structures, could exhibit a dominant-negative effect to impair enzymatic function. Alternatively, start-loss *GLUL* variants could exert a pathogenic effect through stabilization, linked to the loss of glutamine-mediated autoregulation (Figures 3A–3E). To differentiate between these possibilities, the enzymatic activity of the GS_met^{18} was evaluated.

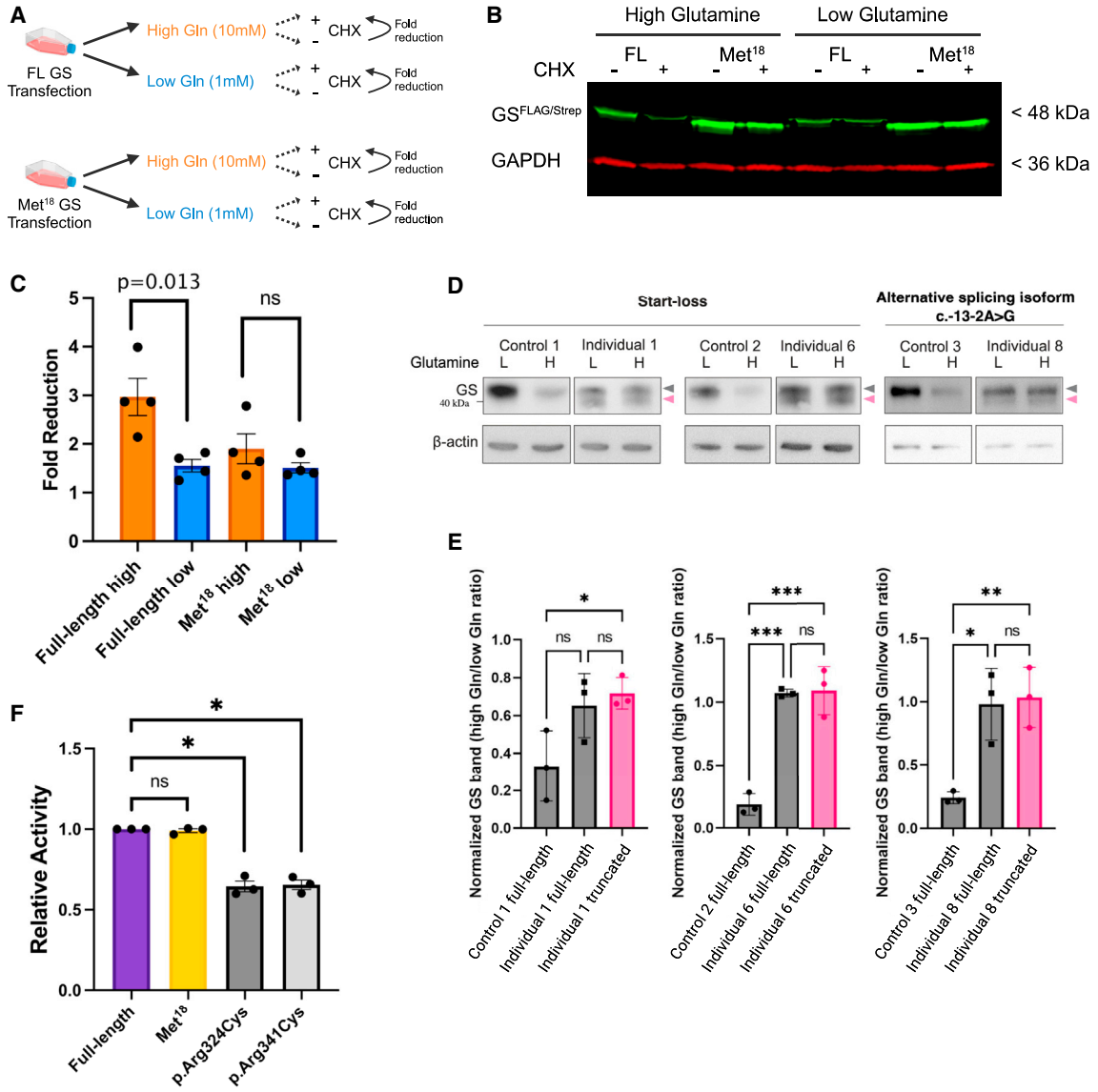

Figure 3. Met[18] GS is stable and full-length GS is unstable in high glutamine conditions

(A) Schematic of cycloheximide assay protocol. Full-length and met[18] GS expression constructs with C-terminal 3xFLAG- Twin-Strep-tags were transfected in HEK293_GLULKO cells. Twelve hours later, a complete media replacement was done with DMEM supplemented with high (10 mM) or low (1 mM) glutamine and treated with 100 μg/ml CHX or DMSO. Cell lysates were sampled after 6 h for western blot analysis with FLAG and GAPDH antibodies. Fold reduction was calculated as the proportion of GS in DMSO treatment relative to CHX treatment.

(B) Western blots of full-length and met[18] GS expression constructs in high and low glutamine. Full-length and met[18] GS expression constructs were transfected into HEK293_GLULKO cells and the protocol outlined in panel A followed (n = 4).

(C) Full-length GS has a significantly higher fold reduction in high glutamine than in low glutamine whereas there is no difference in fold reduction of met[18] GS between high and low glutamine. Following quantification of western blot bands, fold reduction was calculated as the proportion of untreated-to-CHX-treated GS for each glutamine condition. The bar height represents average fold reduction with standard error of the mean presented. Each circle represents a biological replicate. p values were calculated using an unpaired two-tailed Student's t test (n = 4).

(D and E) Subject-derived fibroblasts and age- and sex-matched control fibroblasts were treated with or without 10 mM glutamine for 72 h, and then the protein amount of the full-length GS and the truncated GS were analyzed by quantitative immunoblot. (D) Immunoblot of GS and beta-actin (loading control). Individuals 1 and 6 cells carry a variant at the start codon. Individual 8 cells have a variant that leads to alternative splicing. Controls 1, 2, 3 are the age- and sex-matched control cells. All subject cells express both the full-length (gray arrowheads) and the truncated GS (pink arrowheads). (E) Ratio of the full-length and the truncated GS in the cells cultured with 10 mM glutamine to those cultured without glutamine. The GS band intensity was normalized by the respective beta-actin band control. Gray bars and circles indicate the full-length GS; pink bars and circles indicate the truncated GS. Each circle represents a biological replicate. Error bars indicate standard deviation. Normality was determined with the Shapiro-Wilk test, p values were calculated with a one-way ANOVA, and post-hoc testing was done using the Tukey method (n = 3).

(F) Full-length, met[18], and enzymatically compromised p.Arg324Cys and p.Arg341Cys GS expression constructs were transfected into HEK293_GLULKO cells for enzyme activity measurement. Following affinity purification and buffer exchange, enzymatic activity of

(legend continued on next page)

The catalytic domain of GS lies between amino acid positions 110–358. Notably, GS with the first 22 amino acids truncated can still adopt a stable structure and be incorporated into intact decamers.[27] Consequently, we hypothesized that truncated GS is enzymatically functional. To test this experimentally, a colorimetric activity assay was used to measure the enzymatic activity of GS_FL and GS_met^{18}. Two additional *GLUL* expression constructs with c.970C>T (p.Arg324Cys) and c.1021C>T (p.Arg341Cys) variants were also evaluated as controls. These variants were identified in individuals with autosomal-recessive GS deficiency. The p.Arg324Cys and p.Arg341Cys variants reduce GS enzyme activity to 12% (in immortalized lymphocytes) and 58% (transfected COS7 cells), respectively.[13]

Following transfection of tagged expression constructs, GS_FL, GS_met^{18}, GS_p.Arg324Cys, and GS_p.Arg341Cys were purified and enzymatic activity was determined. When expressed as a proportion of the activity of GS_FL, both enzymatically compromised GS, GS_p.Arg324Cys, and GS_p.Arg341Cys had significantly less activity (GS_p.Arg324Cys 0.64 and GS_p.Arg341Cys 0.65) as previously shown (Figure 3F). The relative activity of GS_met^{18} was not significantly different from that of GS_FL (GS_met^{18} 0.99) (Figure 3F). These data are consistent with published data,[27] indicating that N-terminally truncated GS forms stable, enzymatically active decamers. Overall, these data show that variants initiated at met^{18} lead to a phenotype that results from a loss of negative feedback on GS at the protein level. The retention of GS enzymatic activity indicates that the mechanism underlying this disorder operates through a stabilization mechanism.

GLUL is widely expressed in human neuro- and glial-progenitor cell lineages and in mature glial cell types but not in post-mitotic neurons

Because the primary clinical presentation of this disorder is developmental and epileptic encephalopathy, we sought to identify what cell type(s) expresses *GLUL* during brain development. Using single-nucleus transcriptomic datasets generated from human prefrontal cortex across multiple pre- and post-natal timepoints,[20] we employed uniform manifold approximation and projection (UMAP) clustering to identify previously described cell type clusters including neuronal and glial subtypes (Figure 4Ai). Expression of *GLUL* was substantially higher in glial cell types, primarily astrocytes, compared to other cell clusters including both excitatory and inhibitory neurons (Figure 4Aii and 4Aiii).

To further understand *GLUL* expression during development, single-cell RNA-seq data performed on populations of EGFR$^+$ cells from human cerebral cortex samples were evaluated.[21] Human gliogenesis begins at GW20 corresponding with an increase in EGFR. EGFR$^+$ cells are enriched for glial- and neuronal-lineage progenitors.[21] Following UMAP clustering, *GLUL* expression was found to be constant across glial- and neuronal-progenitor cell type clusters (Figure 4B) and as cortical development progresses *GLUL* expression becomes restricted to the astrocytic lineage.

In addition to *GLUL* expression in neural progenitor cells, one of the individuals studied with a start-loss variant demonstrated periventricular nodular heterotopia as a component of their phenotype, suggesting that dysregulation of *GLUL* could possibly perturb neural progenitor cell proliferation, neuronal differentiation, and/or migration.[28] To examine the effect of the truncated GS on these developmental events, we overexpressed GS_FL or GS_SL under a constitutively active CAG promoter together with EGFP in mouse embryonic cortices using IUE and then analyzed them at the following three time points (Figures S2–S5). Three experiments were performed. In the first, to investigate neural progenitor cell abundance and neuronal-lineage commitment, IUE was performed at E13.5, followed by the analysis at E15.5. In the second, to evaluate gliogenesis, IUE was performed at E16.5, followed by the analysis at E18.5. In the third, to examine the neuronal migration, IUE was performed at E13.5, followed by the analysis at E18.5.

The proportion of GFP$^+$ cells expressing the neural progenitor cell marker protein Pax6 or neuronal lineage-committed progenitor cell marker protein Tbr2 was not significantly changed upon GS_SL overexpression, suggesting that neural progenitor cell abundance, hence neural progenitor cell proliferation and neuronal differentiation were not affected by the production of the truncated GS (Figure S3). Similarly, there were no differences in the proportion of GFP$^+$ cells with Olig2, a gliogenic progenitor cell marker protein, at E18.5 among all experimental groups (Figure S4). The distribution of GFP$^+$ cells, which are the progeny of the electroporated cells at E13.5, in the neocortex at E18.5 did not show any significant changes among all three experimental groups (Figure S5). Therefore, these results do not support a causal relationship between the single observation of periventricular nodular heterotopia and truncated GS.

Discussion

We tentatively propose to name the disorder of glutamine metabolism studied here as glutamine synthetase stabilization disorder (GSSD) and note that it is distinct from the previously described allelic recessive-deficiency disorder.[12–15] This disorder is characterized by a restricted

GS was measured following manufacturer protocols. The enzymatic activity is plotted as a proportion of full-length GS activity. Error bars indicate the standard error of the mean. Each circle represents a biological replicate. p values were calculated using an unpaired two-tailed Student's t test (n = 3). FL, full-length; met^{18}, first 17 amino acids truncated; Gln, glutamine; DMSO, dimethyl sulfoxide; CHX, cycloheximide; *p < 0.05, **p < 0.01, ***p < 0.001, NS, not statistically significant.

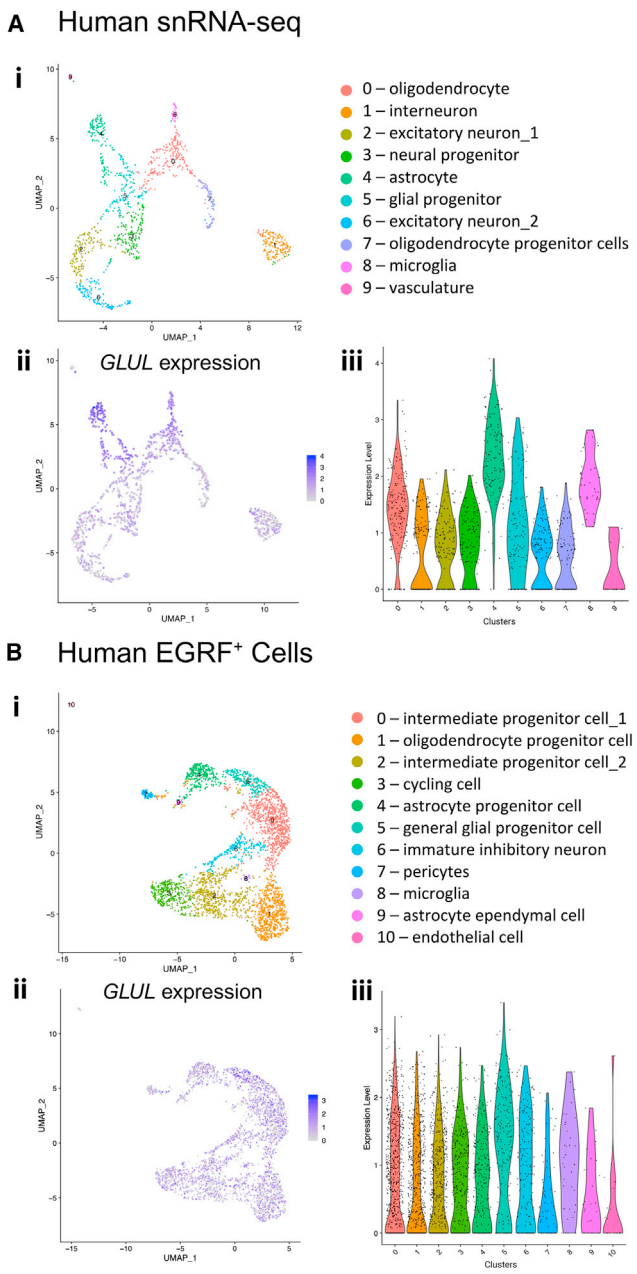

Figure 4. Human cerebral cortex *GLUL* expression at single-cell resolution

(A) Single-nucleus RNA-seq from human prefrontal cortical cells. Data from Herring et al.[20] Samples obtained between mid-gestation (gestational week 22) to adulthood (40 years old).

(i) UMAP of snRNA-seq with 10 cell clusters colored and annotated.

(ii) *GLUL* gene expression overlaid onto UMAP plot of cell clusters.

(iii) Violin plot of *GLUL* expression grouped by cell cluster.

(B) Single-cell RNA-seq from EGRF^{+} cells sampled from human cerebral cortices (between gestational week 21–26). Data from Fu et al.[21]

(i) UMAP of scRNA-seq with 11 cell clusters colored and annotated.

(ii) *GLUL* gene expression overlaid onto UMAP plot of cell clusters.

(iii) Violin plot of *GLUL* expression grouped by cell cluster.

spectrum of causative genetic variants, all of which lead to the loss of the canonical translational initiation codon of *GLUL*. The proteins encoded by the *GLUL* start-loss alleles are stable and enzymatically intact but insensitive to negative feedback via the product of its enzymatic action, glutamine.

There are a small number of described metabolic aminoacidopathies with gain-of-function mechanisms exerting their effects via increased enzymatic activity, prevention of degradation, or blocking inhibition. The disorder resulting from GS stability, as a gain-of-stability aminoacidopathy, is analogous to other disorders that exert dysregulated or overactive enzymatic actions due to loss of allosteric inhibition[2] or an alteration to the active site of the enzyme.[5] The mechanism underlying GS stabilization is the deletion of the degron motif in GS that mediates negative feedback by glutamine. Precedents exist for the causation of disease phenotypes through the stabilization of proteins, principally transcription factors, through impairment of degron motif function.[29,30]

It should be noted that all individuals presented are female. Sex differences in glutamine uptake and metabolism in human gray matter and cultured mouse astrocytes have been described.[31] The molecular basis for this sexual dimorphism in glutamine metabolism may have relevance in the overrepresentation of females in this cohort and possibly alludes to a different, currently uncharacterized, phenotype for males.

Glutamine levels in plasma and cerebrospinal fluid were not consistently elevated as might be anticipated in a disorder characterized by stabilized, active GS. There are conflicting reports on the correlation between plasma, cerebrospinal fluid, brain interstitial fluid, and whole-brain (using magnetic resonance spectroscopy) measurements of glutamine in healthy humans and mice.[32,33] To get a clearer picture of the pathophysiology of this disorder and the role that elevated glutamine might play in its pathophysiology, magnetic resonance spectroscopic measurement of brain glutamine *in vivo* might be an informative and non-invasive method to further investigate this issue in these individuals.[34]

For a condition that acts through stabilization of an otherwise functional enzyme, corresponding enzymatic inhibitors represent a plausible class of agent to consider as treatment. Methionine sulfoximine (MSO), an irreversible GS inhibitor, has potential as a therapeutic agent and has been trialed in mammalian models of hyperammonemic encephalopathy. In hyperammonemic syndromes, there is an increase in cerebral and cerebrospinal fluid glutamine due to an increase in astrocytic GS activity, functioning as the primary method of ammonia fixation in the brain. A predominant theory of pathogenesis of hyperammonemic encephalopathy, the osmotic gliopathy hypothesis, associates increased glutamine (rather than hyperammonia, per se) with astrocytic osmotic imbalance and astrocyte swelling.[35] A similar mechanism may be operative in the encephalopathy associated with the disorder described here. MSO has successfully been trialed as a therapeutic intervention in hyperammonemic rats, preventing or attenuating several

neuropathological changes when administered at subconvulsant doses.[35–37]

Questions remain, however, around the toxicity of metabolic products of MSO, off-target effects, interspecies differences in its potency, and its propensity to induce seizures.

The *de novo* start-loss variants in *GLUL* result in a developmental and epileptic encephalopathy with intractable seizures. A variety of pathogenic mechanisms could underlie this presentation including dysregulated neurotransmitter metabolism, removal of ammonia, astrocytic swelling due to osmotic stress, altered mitochondrial energetics, and consumption of ATP.

As a major mechanism for the removal of ammonia in the brain, stabilization of GS in individuals with this disorder could conceivably lead to metabolic imbalance resulting in disturbance of pH and nitrogen flux in the central nervous system. As would be predicted, no abnormalities of systemic pH, ammonia, or glutamine levels were noted in any individual in this study, likely because the liver and other non-central nervous system tissues have compensatory pathways for such metabolic dysfunction. What is clear is that even if GS stabilization has its primary origins as a disorder of glial cells in the brain, the metabolic consequences of dysregulated GS activity for neuronal functions are likely to be more broadly dispersed over other cell types.

A newly recognized role for glutamine in the developing brain has recently been highlighted with glutaminolysis being shown to influence mitochondrial energetics, neural progenitor cell abundance, and proliferation during human fetal development.[11,38] Glutaminolysis is a catabolic process that converts glutamine to glutamate and then in turn to α-ketoglutarate, which is metabolized through the tricarboxylic acid cycle. Glutaminolysis is a metabolic characteristic of human fetal neural progenitor cells, particularly basal progenitors, which are notably abundant in the human cerebral cortex. The influence of stabilized GS on glutaminolysis may be human specific as this metabolic pathway is activated by a human-specific protein ARHGAP11B.[11,39] It is conceivable that in individuals with this disorder, the constitutively active GS consumes glutamate to produce glutamine, thereby suppressing glutaminolysis that may otherwise influence the proliferation of neural progenitor cells in the human fetal neocortex.

GS consumes ATP to convert glutamate to glutamine. Stabilized GS may constitutively reduce levels of ATP in the cells expressing *GLUL* (e.g., astrocytes). ATP acts not only as an energy source but also acts in intracellular signaling. Secreted ATP from astrocytes inhibits excitatory synaptic transmission as well as enhances inhibitory GABAergic inputs onto excitatory neurons.[40] A reduction of ATP in astrocytes might contribute to an imbalance in excitatory/inhibitory synaptic transmission and consequently the epileptic phenotype in this disorder. Additionally, extracellular ATP is known to promote myelination.[41] Because the present results suggest that there are no changes in the abundance of the gliogenic progenitor cells in the developing cerebral cortex, the hypomyelination phenotype might be contributed to by insufficient ATP secretion from astrocytes.

Start-loss variants in GS may exert effects independent of its canonical enzymatic activity. Recently, it was found that GS interacts with and sustains GTPase RHOJ palmitoylation, thereby mediating membrane localization and activation of RHOJ. The effect of this is reduced vessel sprouting, increased actin stress fibers, and impaired endothelial cell motility.[42] Conceivably, this accessory function of GS in modulating angiogenesis and cytoskeletal remodeling could influence human neurodevelopment.

The allelic disorders of GS deficiency disorder and GS stabilization both illustrate the importance of tight homeostatic regulation of glutamine during human fetal neurodevelopment. The derangement of metabolism that results as a consequence of these enzymatic defects could stem from multiple mechanisms that must be considered when evaluating therapeutic approaches to treat these conditions.

Data and code availability

The accession numbers for *GLUL* variants reported in this paper are ClinVar: SCV004177219–SCV004177224.

The whole-exome sequence data supporting the current study have not been deposited in a public repository to preserve the confidentiality and privacy of the participants but are available from the corresponding author on request.

Supplemental information

Supplemental information can be found online at https://doi.org/10.1016/j.ajhg.2024.03.005.

Acknowledgments

The authors would like to acknowledge the participants and their families for their participation in this work.

We thank the Center of Protein Research, University of Otago for mass spectrometry expertise provided by Torsten Kleffmann. We also thank the Biomedicum Imaging Unit, *in vivo* Brain Imaging Unit, and Laboratory Animal Center of the University of Helsinki for their excellent services and E. Huttu and S. Lågas for technical assistance.

S.P.R. is supported by CureKids. T.N. is supported by the Research Council of Finland (340179, 351966), ERA-NET NEURON (MEPIcephaly), the Sigrid Jusélius Foundation, the Brain Science Foundation, and HiLIFE Fellow program at the University of Helsinki and is partially supported by the profiling area Understanding the Human Brain (UHBRAIN) of PROFI 6 Competitive funding to strengthen university research profiles, granted by the Research Council of Finland to the University of Helsinki (336234). This work was also supported in part by Telethon Undiagnosed Diseases Program (TUDP, GSP15001).

Author contributions

Conceptualization: S.P.R., L.D., H.R.U., T.N., Z.J., and A.G.J.
Data curation: L.D., H.R.U., R.J.T., G.G., and A.G.J.
Resources: R.J.T., L.D., G.L.C., S.J.D., D.K.G., M.J.H., M.H.-E., J.H., S.M., V.N., M.M., V.P., C.S., A.I.E., T.P., A.S., J.A.P., H.R.U., and S.P.R.
Investigation, formal analysis, and visualization: A.G.J., M.A., B.J.H., I.G.-L., A.K., Z.J., G.G., T.N., and S.P.R.
Supervision: S.P.R., Z.J., T.N., and G.G.
Writing – original draft: A.G.J., S.P.R., T.N., Z.J., and M.A.
Writing – review and editing: all authors.

Declaration of interests

The authors declare no competing interests.

Received: December 19, 2023
Accepted: March 6, 2024
Published: April 4, 2024

References

1. Ferreira, C.R., van Karnebeek, C.D.M., Vockley, J., and Blau, N. (2019). A proposed nosology of inborn errors of metabolism. Genet. Med. *21*, 102–106.
2. Palladino, A.A., and Stanley, C.A. (2010). The hyperinsulinism/hyperammonemia syndrome. Rev. Endocr. Metab. Disord. *11*, 171–178.
3. Tsuchida, N., Hamada, K., Shiina, M., Kato, M., Kobayashi, Y., Tohyama, J., Kimura, K., Hoshino, K., Ganesan, V., Teik, K.W., et al. (2018). GRIN2D variants in three cases of developmental and epileptic encephalopathy. Clin. Genet. *94*, 538–547.
4. Li, D., Yuan, H., Ortiz-Gonzalez, X.R., Marsh, E.D., Tian, L., McCormick, E.M., Kosobucki, G.J., Chen, W., Schulien, A.J., Chiavacci, R., et al. (2016). GRIN2D Recurrent De Novo Dominant Mutation Causes a Severe Epileptic Encephalopathy Treatable with NMDA Receptor Channel Blockers. Am. J. Hum. Genet. *99*, 802–816.
5. Rumping, L., Tessadori, F., Pouwels, P.J.W., Vringer, E., Wijnen, J.P., Bhogal, A.A., Savelberg, S.M.C., Duran, K.J., Bakkers, M.J.G., Ramos, R.J.J., et al. (2019). GLS hyperactivity causes glutamate excess, infantile cataract and profound developmental delay. Hum. Mol. Genet. *28*, 96–104.
6. Watson, L.M., Bamber, E., Schnekenberg, R.P., Williams, J., Bettencourt, C., Lickiss, J., Jayawant, S., Fawcett, K., Clokie, S., Wallis, Y., et al. (2017). Dominant Mutations in GRM1 Cause Spinocerebellar Ataxia Type 44. Am. J. Hum. Genet. *101*. 866–458.
7. Bak, L.K., Schousboe, A., and Waagepetersen, H.S. (2006). The glutamate/GABA-glutamine cycle: aspects of transport, neurotransmitter homeostasis and ammonia transfer. J. Neurochem. *98*, 641–653.
8. Hayashi, M.K. (2018). Structure-Function Relationship of Transporters in the Glutamate-Glutamine Cycle of the Central Nervous System. Int. J. Mol. Sci. *19*, 1177.
9. Zhou, Y., Eid, T., Hassel, B., and Danbolt, N.C. (2020). Novel aspects of glutamine synthetase in ammonia homeostasis. Neurochem. Int. *140*, 104809.
10. Yoo, H.C., Yu, Y.C., Sung, Y., and Han, J.M. (2020). Glutamine reliance in cell metabolism. Exp. Mol. Med. *52*, 1496–1516.
11. Namba, T., Dóczi, J., Pinson, A., Xing, L., Kalebic, N., Wilsch-Bräuninger, M., Long, K.R., Vaid, S., Lauer, J., Bogdanova, A., et al. (2020). Human-Specific ARHGAP11B Acts in Mitochondria to Expand Neocortical Progenitors by Glutaminolysis. Neuron *105*, 867–881.e9.
12. Spodenkiewicz, M., Diez-Fernandez, C., Rüfenacht, V., Gemperle-Britschgi, C., and Häberle, J. (2016). Minireview on Glutamine Synthetase Deficiency, an Ultra-Rare Inborn Error of Amino Acid Biosynthesis. Biology *5*, 40.
13. Häberle, J., Görg, B., Rutsch, F., Schmidt, E., Toutain, A., Benoist, J.F., Gelot, A., Suc, A.L., Höhne, W., Schliess, F., et al. (2005). Congenital glutamine deficiency with glutamine synthetase mutations. N. Engl. J. Med. *353*, 1926–1933.
14. Häberle, J., Shahbeck, N., Ibrahim, K., Hoffmann, G.F., and Ben-Omran, T. (2011). Natural course of glutamine synthetase deficiency in a 3year old patient. Mol. Genet. Metabol. *103*, 89–91.
15. Ünal, Ö., Ceylaner, S., and Akın, R. (2019). A Very Rare Etiology of Hypotonia and Seizures: Congenital Glutamine Synthetase Deficiency. Neuropediatrics *50*, 051–053.
16. He, Y., Hakvoort, T.B.M., Vermeulen, J.L.M., Lamers, W.H., and Van Roon, M.A. (2007). Glutamine synthetase is essential in early mouse embryogenesis. Dev. Dynam. *236*, 1865–1875.
17. Nguyen, T.V., Lee, J.E., Sweredoski, M.J., Yang, S.J., Jeon, S.J., Harrison, J.S., Yim, J.H., Lee, S.G., Handa, H., Kuhlman, B., et al. (2016). Glutamine Triggers Acetylation-Dependent Degradation of Glutamine Synthetase via the Thalidomide Receptor Cereblon. Mol. Cell *61*, 809–820.
18. Sobreira, N., Schiettecatte, F., Valle, D., and Hamosh, A. (2015). GeneMatcher: a matching tool for connecting investigators with an interest in the same gene. Hum. Mutat. *36*, 928–930.
19. Chin, C.L., Goh, J.B., Srinivasan, H., Liu, K.I., Gowher, A., Shanmugam, R., Lim, H.L., Choo, M., Tang, W.Q., Tan, A.H.-M., et al. (2019). A human expression system based on HEK293 for the stable production of recombinant erythropoietin. Sci. Rep. *9*, 16768.
20. Herring, C.A., Simmons, R.K., Freytag, S., Poppe, D., Moffet, J.J.D., Pflueger, J., Buckberry, S., Vargas-Landin, D.B., Clément, O., Echeverría, E.G., et al. (2022). Human prefrontal cortex gene regulatory dynamics from gestation to adulthood at single-cell resolution. Cell *185*, 4428–4447.e28.
21. Fu, Y., Yang, M., Yu, H., Wang, Y., Wu, X., Yong, J., Mao, Y., Cui, Y., Fan, X., Wen, L., et al. (2021). Heterogeneity of glial progenitor cells during the neurogenesis-to-gliogenesis switch in the developing human cerebral cortex. Cell Rep. *34*, 108788.
22. Stuart, T., Butler, A., Hoffman, P., Hafemeister, C., Papalexi, E., Mauck, W.M., Hao, Y., Stoeckius, M., Smibert, P., and Satija, R. (2019). Comprehensive Integration of Single-Cell Data. Cell *177*, 1888–1902.e21.
23. Butler, A., Hoffman, P., Smibert, P., Papalexi, E., and Satija, R. (2018). Integrating single-cell transcriptomic data across different conditions, technologies, and species. Nat. Biotechnol. *36*, 411–420.
24. Namba, T., Kibe, Y., Funahashi, Y., Nakamuta, S., Takano, T., Ueno, T., Shimada, A., Kozawa, S., Okamoto, M., Shimoda, Y., et al. (2014). Pioneering axons regulate neuronal polarization in the developing cerebral cortex. Neuron *81*, 814–829.
25. Heinzen, E.L., O'Neill, A.C., Zhu, X., Allen, A.S., Bahlo, M., Chelly, J., Chen, M.H., Dobyns, W.B., Freytag, S., Guerrini, R., et al. (2018). De novo and inherited private variants in

MAP1B in periventricular nodular heterotopia. PLoS Genet. *14*, e1007281.
26. Jaganathan, K., Kyriazopoulou Panagiotopoulou, S., McRae, J.F., Darbandi, S.F., Knowles, D., Li, Y.I., Kosmicki, J.A., Arbelaez, J., Cui, W., Schwartz, G.B., et al. (2019). Predicting Splicing from Primary Sequence with Deep Learning. Cell *176*, 535–548.e24.
27. Chek, M.F., Kim, S.-Y., Mori, T., Kojima, H., and Hakoshima, T. (2021). Crystal structure of N-terminal degron-truncated human glutamine synthetase. Acta Crystallogr. F *77*, 427–434.
28. Battaglia, G., and Granata, T. (2007). Periventricular nodular heterotopia. In Handbook of Clinical Neurology (Elsevier), pp. 177–189.
29. Acuna-Hidalgo, R., Deriziotis, P., Steehouwer, M., Gilissen, C., Graham, S.A., van Dam, S., Hoover-Fong, J., Telegrafi, A.B., Destree, A., Smigiel, R., et al. (2017). Overlapping SETBP1 gain-of-function mutations in Schinzel-Giedion syndrome and hematologic malignancies. PLoS Genet. *13*, e1006683.
30. Voisin, N., Schnur, R.E., Douzgou, S., Hiatt, S.M., Rustad, C.F., Brown, N.J., Earl, D.L., Keren, B., Levchenko, O., Geuer, S., et al. (2021). Variants in the degron of AFF3 are associated with intellectual disability, mesomelic dysplasia, horseshoe kidney, and epileptic encephalopathy. Am. J. Hum. Genet. *108*, 857–873.
31. Sponagel, J., Jones, J.K., Frankfater, C., Zhang, S., Tung, O., Cho, K., Tinkum, K.L., Gass, H., Nunez, E., Spitz, D.R., et al. (2022). Sex differences in brain tumor glutamine metabolism reveal sex-specific vulnerabilities to treatment. Méd. *3*, 792–811.e12.
32. Takado, Y., Sato, N., Kanbe, Y., Tomiyasu, M., Xin, L., Near, J., Yoshikawa, K., Sahara, N., Higashi, T., Suhara, T., et al. (2019). Association between Brain and Plasma Glutamine Levels in Healthy Young Subjects Investigated by MRS and LC/MS. Nutrients *11*, 1649.
33. Dolgodilina, E., Imobersteg, S., Laczko, E., Welt, T., Verrey, F., and Makrides, V. (2016). Brain interstitial fluid glutamine homeostasis is controlled by blood–brain barrier SLC7A5/LAT1 amino acid transporter. J. Cerebr. Blood Flow Metabol. *36*, 1929–1941.
34. Ramadan, S., Lin, A., and Stanwell, P. (2013). Glutamate and glutamine: a review of in vivo MRS in the human brain. NMR Biomed. *26*, 1630–1646.
35. Brusilow, S.W., Koehler, R.C., Traystman, R.J., and Cooper, A.J.L. (2010). Astrocyte Glutamine Synthetase: Importance in Hyperammonemic Syndromes and Potential Target for Therapy. Neurotherapeutics *7*, 452–470.
36. Brusilow, W.S.A., and Peters, T.J. (2017). Therapeutic effects of methionine sulfoximine in multiple diseases include and extend beyond inhibition of glutamine synthetase. Expert Opin. Ther. Targets *21*, 461–469.
37. Jeitner, T.M., and Cooper, A.J.L. (2014). Inhibition of human glutamine synthetase by L-methionine-S,R-sulfoximine-relevance to the treatment of neurological diseases. Metab. Brain Dis. *29*, 983–989.
38. Namba, T., Nardelli, J., Gressens, P., and Huttner, W.B. (2021). Metabolic Regulation of Neocortical Expansion in Development and Evolution. Neuron *109*, 408–419.
39. Florio, M., Albert, M., Taverna, E., Namba, T., Brandl, H., Lewitus, E., Haffner, C., Sykes, A., Wong, F.K., Peters, J., et al. (2015). Human-specific gene ARHGAP11B promotes basal progenitor amplification and neocortex expansion. Science *347*, 1465–1470.
40. Lezmy, J. (2023). How astrocytic ATP shapes neuronal activity and brain circuits. Curr. Opin. Neurobiol. *79*, 102685.
41. Ishibashi, T., Dakin, K.A., Stevens, B., Lee, P.R., Kozlov, S.V., Stewart, C.L., and Fields, R.D. (2006). Astrocytes Promote Myelination in Response to Electrical Impulses. Neuron *49*, 823–832.
42. Eelen, G., Dubois, C., Cantelmo, A.R., Goveia, J., Brüning, U., DeRan, M., Jarugumilli, G., van Rijssel, J., Saladino, G., Comitani, F., et al. (2018). Role of glutamine synthetase in angiogenesis beyond glutamine synthesis. Nature *561*, 63–69.